Development and application of an interface constitutive model for fully grouted rock-bolts and cable-bolts

Emad Jahangir, Laura Blanco Martín, Faouzi Hadj-Hassen, Michel Tijani

Development and application of an interface constitutive model for fully grouted rock-bolts and cable-bolts

Emad Jahangir*, Laura Blanco-Martín, Faouzi Hadj-Hassen, Michel Tijani

MINES ParisTech, PSL Research University, Department of Geosciences, 35 rue Saint Honoré, 77300 Fontainebleau, France

ARTICLEINFO

Article history:
Received 1 September 2020
Received in revised form
2 February 2021
Accepted 7 March 2021
Available online

Keywords:
Fully grouted bolts
Interface constitutive model
Dilatancy
Pull-out tests
Finite element method (FEM) modeling

ABSTRACT

This paper proposes a new interface constitutive model for fully grouted rock-bolts and cable-bolts based on pull-out test results. A database was created combining published experimental data with in-house tests. By means of a comprehensive framework, a Coulomb-type failure criterion accounting for friction mobilization was defined. During the elastic phase, in which the interface joint is not yet created, the proposed model provides zero radial displacement, and once the interface joint is created, interface dilatancy is modeled using a non-associated plastic potential inspired from the behavior of rock joints. The results predicted by the proposed model are in good agreement with experimental results. The model has been implemented in a finite element method (FEM) code and numerical simulations have been performed at the elementary and the structural scales. The results obtained provide confidence in the ability of the new model to assist in the design and optimization of bolting patterns.

1. Introduction

Fully grouted rock-bolts and cable-bolts are two reinforcement systems for rock stabilization, both in mining and civil engineering applications. Due to their ease of installation, low cost, minimal space taken in an excavation, adaptability and high load-bearing capacity, they are extensively used in underground excavations (Stillborg, 1986; Li, 2017). Fully grouted bolts consist of four elements (Windsor and Thompson, 1996): the surrounding ground (rock or soil), the reinforcing bar (rock-bolt or cable-bolt), the internal fixture to the borehole wall (grouting material) and the external fixture to the excavation surface (typically, a plate and a nut).

Fully grouted bolts can hold tensile, compressive, shear and bending loads, which leads to complex loading configurations in the field. In order to gain more insight into the load transfer mechanism between the bolt and the surrounding ground, it is necessary to assess the response of the bolt-grout and the grout-ground interfaces. Previous studies prove that, when the surrounding ground is rock, failure of fully grouted bolts often occurs along the bolt-grout interface, by means of a debonding process that starts at the point where the load is applied and progressively propagates along the interface (e.g. Blanco-Martín, 2012). According to Li and Stillborg (1999), the interface bond is provided by three mechanisms: adhesion, mechanical interlock and friction; these mechanisms are lost progressively as debonding of the interface occurs. The behavior of the bolt-grout interface is still a key issue for the stability assessment of rock engineering structures.

In order to study the bolt-grout interface, axial loading conditions are used (pull-out test configuration, see Fig. 1, in which a vertical upward displacement is applied to the bolt, while the grout and the ground are fixed). The embedment length used should allow for debonding before the yield strength of the bolt is reached. Once the force on the bolt is large enough, the shear stress on the interface locally exceeds the shear strength, and debonding between the bolt and the grout occurs. Debonding starts at the loaded end of the bar and propagates towards the free end. During this process, the interface switches from a continuous medium to a discontinuous medium, which involves the creation of a joint between the bolt and the grout. Before debonding, there is no relative slip between the bar and the grouting material, and the interface is closed in the radial direction; after debonding, the opposite is true. Given the geometry of the problem, radial (or normal) and tangential (or axial) directions take part in the interface response, and rotational invariance is often assumed.

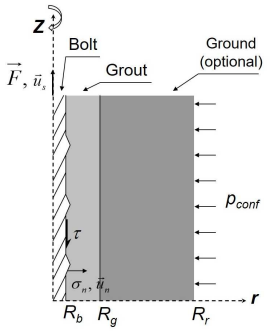

Fig. 1. Schematic representation of the pull-out configuration.

Hyett et al. (1992) studied the effect of the confining pressure on the bond strength of fully grouted cable-bolts and highlighted its importance on the interface behavior. Later, Hyett et al. (1995) proposed a constitutive law for cement-grouted seven-wire cable-bolts, without considering the debonding process (i.e. the model can only be applied after decoupling of the interface has occurred). This law assumes that the shear stress is purely frictional and independent of the axial slip (except for untwisting). Regarding the normal response, a hyperbolic dilatant opening was assumed, adapted from nonlinear rock joints. The comparison between experimental and modeled pull-out tests using this law is in general quite satisfactory. However, the law is only valid after debonding and its ability to describe the bolt-grout interface of rock-bolts has not been discussed in published communications. Moosavi et al. (2005) studied the effect of the confining pressure on rock-bolts under constant radial pressure, using the same device as Hyett et al. (1995). They reported the importance of the normal stress acting on the rebar, highlighting the frictional nature of the bond, but no constitutive law was proposed for the interface.

Overall, the literature review shows that the models dealing with fully grouted bolts are generally based either on the bond-slip model

*Corresponding author. E-mail address: emad.jahangir@mines-paristech.fr

or on constitutive laws derived from rock joint models. The first category combines the stress equilibrium along the bolt with an often-empirical shear stress-slip relationship, and the radial behavior is not considered explicitly (Benmokrane et al., 1995; Li and Stillborg, 1999). This approach has been handled by numerical methods (Cai et al., 2004; Chen et al., 2015a; Ma et al., 2016) as well as analytical methods (Nairn, 2004; Ren et al., 2010; Blanco-Martín et al., 2011; He et al., 2014; Chen et al., 2015b). Regarding the second category, rock joint constitutive models use friction mobilization or cohesion degradation depending on the characteristics of the rock and the interface. Friction angle mobilization (related to the mobilized asperity angle) has been extensively used in the literature, including works on reinforcement elements (Ladanyi and Archambault, 1980; Plesha, 1987; Barton and Bandis, 1990; Saeb and Amadei, 1992; Alejano and Alonso, 2005; Indraratna et al., 2015; Oh et al., 2015; Li et al., 2017). There also exists the cohesion degradation concept used for cohesive fracture of quasi-brittle materials (Carol et al., 1997; Pouya and Yazdi, 2015; Renani and Martin, 2018) and for composite elements with a cohesive interface (Chen et al., 2015b; Tian et al., 2015). Within this second category, Li et al. (2017) developed a model for modified geometry cable-bolts including a peak axial load envelope given by an empirical relationship proposed by Ladanyi and Archambault (1980). This model, based on Hyett et al. (1995)'s model, assumes that the major contribution to the bond strength is the mobilized friction between the bulge and the grout. The comparison between model predictions and experimental results is quite satisfactory, but the model has not been numerically implemented to perform structural scale computations. The importance of friction was also highlighted in studies of Blanco-Martín et al. (2013, 2016), who proposed a semi-empirical model for steel and fiberglass reinforced polymer (FRP) rock-bolts grouted with resin grouts; however, a major limitation of this model is that it does not account explicitly for debonding (i.e. there is no yield criterion). Cui et al. (2019a) highlighted the importance of slip (debonding) for rock-bolts and concluded that for both soft and hard surrounding rocks, the non-slip case is severely conservative for rock-bolt design.

This study aims to present a new interface constitutive model applicable to both rock-bolts and cable-bolts, and able to predict the axial and the radial responses of the interface with a reduced number of parameters. The model is established based on laboratory-scale pull-out tests and includes debonding. It adopts the friction angle mobilization concept used for rock joints because it can handle the different responses of rock-bolts and cable-bolts to debonding: while the former shows significant softening, the latter is characterized by hardening or a quasi-constant post-peak response. We first present the new model and explain how to estimate parameters from experimental data. Then, the predictions of the new model in the axial and radial directions are compared with experimental pull-out test results. A database with in-house and literature results has been created for this purpose. In the last section, details of the model implementation in a finite element method (FEM) code are given, and simulation results of pull-out tests at the elementary and the structural scales are shown and compared with experimental data. The satisfactory results obtained provide confidence in the ability of the new model to assist in the design and optimization of bolting patterns.

2. New constitutive model

2.1. Preliminary definitions

Let $\vec{u} = \vec{u}_b - \vec{u}_g$ be the relative displacement vector at the interface between the bolt and the grout, where $\vec{u}_b$ and $\vec{u}_g$ are the bolt and grout displacements, respectively. Vector $\vec{u}$ has a normal component, $u_n = \vec{u}\vec{n}$, where $\vec{n}$ is the unit outward-pointing normal vector. The shear or tangential displacement vector is $\vec{u}_s = \vec{u} - u_n\vec{n}$. In the following, compression and closure are assumed to be negative.

Let $\vec{s} = \underline{\underline{\sigma}}_b \vec{n}$ be the stress vector at the interface, where $\underline{\underline{\sigma}}_b$ is the stress tensor in the bolt. We note that $\underline{\underline{\sigma}}_b \vec{n} = \underline{\underline{\sigma}}_g \vec{n}$. The stress vector has a normal component, $\sigma_n = \vec{s}\,\vec{n}$, and a shear component, $\vec{\tau} = \vec{s} - \sigma_n \vec{n}$. The unit tangential vector is $\vec{t} = \vec{\tau}/\|\vec{\tau}\|$.

The interface is assumed to be elastoplastic and to obey to the incremental law:

$$\left.\begin{aligned} \delta u_n &= \frac{\delta\sigma_n}{K_n} + \delta u_n^p \\ \delta \vec{u}_s &= \frac{\delta\vec{\tau}}{K_s} + \delta \vec{u}_s^p \end{aligned}\right\} \quad (1)$$

where K_n and K_s are the normal and shear stiffness of the interface, respectively; and $\vec{u^p} = \vec{u_s^p} + u_n^p \vec{n}$ is the plastic relative displacement at the interface. The plastic shear displacement increment vector is $\delta \vec{u}_s^p = \delta\xi\, \vec{t}$, where the internal variable verifies $\delta\xi \geq 0$.

2.2. Failure criterion and plastic potential

Failure of the interface is reached by an excess of shear stress. A non-elastic normal response can occur only after failure; this implies $\delta u_n^p = \psi(\sigma_n, \xi)\delta\xi$, where ψ is a known function.

The admissible stress states must verify the following inequality (Khan and Huang, 1995; Chakrabarty, 2006):

$$f(\vec{s}, \xi) = \tau - \varphi(\sigma_n, \xi) \leq 0 \quad (2)$$

where $\tau = \|\vec{\tau}\|$. As long as $f < 0$, the interface behavior is linear elastic and reversible, so that we have

$$\delta\vec{u} = \frac{\delta\vec{\tau}}{K_s} + \frac{\delta\sigma_n}{K_n}\vec{n} \quad (3)$$

When $f = 0$, plastic flow occurs with $\delta\xi > 0$ and an increment of displacement is given by

$$\delta \vec{u} = \frac{\delta\vec{\tau}}{K_s} + \frac{\delta\sigma_n}{K_n}\vec{n} + \delta\xi\,(\vec{t} + \psi(\sigma_n, \xi)\,\vec{n}) \quad (4)$$

From Eq. (4), the increment of axial displacement can be expressed as

$$\delta u_s = \frac{\delta\tau}{K_s} + \delta\xi \quad (5)$$

where $u_s = \|\vec{u_s}\|$. Since at failure, $\tau = \varphi\,(\sigma_n, \xi)$ (Eq. 2), it comes that

$$\delta\tau = \partial_\xi\varphi\ \delta\xi \quad (6)$$

From Eqs. (5) and (6), it can be deduced that

$$\delta u_s = \left(\frac{\partial_\xi\varphi}{K_s} + 1\right)\delta\xi \quad (7)$$

where $\partial_\xi\varphi$ means derivative of φ regarding to ξ argument.

Since $\delta u_s > 0$ and $\delta\xi > 0$, we obtain the following condition for function $\varphi(\sigma_n, \xi)$:

$$\frac{\partial_\xi\varphi}{K_s} + 1 > 0 \quad (8)$$

The plastic potential (non-associated flow rule) is given by

$$P(\vec{s}, \xi) = \tau - \overline{\psi}(\sigma_n, \xi) \quad (9)$$

where

$$\overline{\psi}(\sigma_n, \xi) = \int_0^{\sigma_n}[-\psi(\sigma_n, \xi)]\mathrm{d}\sigma \quad (10)$$

According to the normality rule (Lubliner, 2008), any plastic displacement increment must verify:

$$\delta\vec{u^p} = \delta\xi\partial_{\vec{s}}P = \delta\xi(\vec{t} - \partial_{\sigma_n}\overline{\psi}\vec{n}) \quad (11)$$

The comparison between the plastic part of Eqs. (4) and (11) shows that, instead of the full expression of the potential (Eq. (9)), only $\psi = -\partial_{\sigma_n}\overline{\psi}$ is needed.

To sum up, the interface is defined by the stress vector $\vec{s}$ and the internal variable ξ. The elastic response is defined by two constants (K_n and K_s) and the plastic response (active if the shear strength of the interface is reached) is defined by functions $\varphi(\sigma_n, \xi)$ (with $\partial_\xi \varphi + K_s > 0$) and $\psi(\sigma_n, \xi)$.

For one increment of interface evolution, the plastic work is given by (Hill, 1948):

$$\delta w^p = \vec{s}\delta\vec{u}^p = (\varphi + \sigma_n\psi)\delta\xi \quad (12)$$

Since $\delta w^p > 0$ and given that $\delta\xi > 0$, functions φ and ψ must verify:

$$\forall\,(\sigma_n, \xi),\ \varphi(\sigma_n, \xi) + \sigma_n\psi(\sigma_n, \xi) \geq 0 \quad (13)$$

The above condition imposes some constraints on the functions and model parameters. For instance, for the Mohr-Coulomb criterion ($\varphi = c - \sigma_n \tan\phi$ and $\psi = \tan\Psi$, where ϕ and Ψ are the fraction and dilatancy angles, respectively), Eq. (13) imposes the well-known conditions $c \geq 0$ and $\Psi \leq \phi$, and it comes that the friction and dilatancy angles should be in the range $[0, \pi/2[$.

It should be noted that the framework described above is suitable to determine any appropriate yield criterion and plastic potential for the interface, as long as Eq. (2) and the conditions given by Eqs. (8) and (13) are satisfied. In order to complete this general methodology, we explain next how to determine parameters and necessary functions from pull-out test results.

2.3. Derivation of model parameters from laboratory-scale pull-out test results

In a pull-out test, the interface is first coupled (i.e. there is no relative displacement between the bolt and the grout), and at an early stage progressive debonding occurs as a discontinuity is created along the interface (Blanco-Martín, 2012). This joint creation shifts the interface response from continuous to discontinuous and should be included in the constitutive model of the interface.

In practice, in a pull-out test, a displacement is applied normal to the cross-section of the bolt and a compressive stress is applied normal to the interface (see Fig. 1). If the test is correctly instrumented, the normal pressure, the shear stress, the normal displacement and the shear displacement can be determined at the interface. It should be noted that depending on the experimental conditions, it might be difficult to determine these variables (for example, the shear stress is not uniform if the embedment length is long). When these variables are available from pull-out tests, the following operations should be carried out to determine K_n, K_s, φ and ψ:

(1) The shear stiffness (assumed independent of σ_n) can be derived from the initial linear phase of the test, which is assumed to be elastic and reversible.

(2) The scalar internal variable can be computed using $\xi = u_s^p = u_s - \tau/K_s$, and then function $\varphi(\sigma_n, \xi)$ can be determined.

(3) The plastic normal displacement can be computed using $u_n^p = u_n - \sigma_n/K_n$. In this work, the interface is assumed to have no elastic component in the normal direction, and consequently K_n is chosen very large, so that $u_n^p \approx u_n$. Additionally, it can be inferred from Eq. (4) that $\mathrm{d}u_n^p/\mathrm{d}\xi = \psi(\sigma_n, \xi)$.

2.4. New interface model

The new interface constitutive model comprises a failure criterion and a plastic potential that should be verified using Eqs. (2), (8) and (13). Based on experimental results, the cohesion is degraded rapidly with the axial displacement for rock-bolts, although some residual cohesion remains at the end of the test (e.g. Blanco-Martín et al., 2013; Tian et al., 2015). For cable-bolts, there is no significant load drop, reflecting little cohesion degradation (Hyett et al., 1995; Thenevin et al., 2017). Experimental determination of this cohesion degradation is very complex; in turn, friction is likely present throughout the entire test (Li and Stillborg, 1999). For this reason, the friction angle mobilization concept is adopted in the new model. As it will be seen, the model can handle both hardening (cable-bolts) and softening (rock-bolts) behaviors with proper parameters. The different shear response of rock-bolts and cable-bolts, observed systematically in experiments, finds its origin in the different bolt geometries (plain bar vs. twisted wires) as well as in the roughness of the bolt indentations. As for rock-bolts, the indentations are generally taller and rougher, so the interface is degraded rapidly and the shear strength drops to a residual value when debonding occurs. As for cable bolts, the indentations are usually smaller and smoother, leading to a much more progressive interface degradation, and, before failure, the interface shear strength is mobilized, leading to hardening.

2.5. Axial behavior

Let us define $\varphi(\sigma_n, \xi) = c_r - \sigma_n\phi(\xi)$, where c_r is the residual cohesion, and $\phi(\xi)$ is an empirical function accounting for the variation of the friction angle as a function of the internal variable ξ:

$$\phi(\xi) = \left(m\sqrt{\frac{\xi}{w_c^p}} + n\right)\exp\left(-\frac{\xi}{w_c^p}\right) + k \quad (14)$$

Function $\phi(\xi)$ is defined by four parameters: m, n, k and w_c^p, that must satisfy Eq. (8). The critical plastic axial displacement, w_c^p, is an intrinsic value of the interface and is independent of the confining pressure. It depends only on the interlock characteristics (grout quality and bolt type). Hardening of the interface occurs between the elastic displacement limit, w_c^e (end of straight line in Fig. 2), and $\xi = \left[(m^2+n^2)w_c^p \pm \sqrt{n^2(2m^2+n^2)(w_c^p)^2}\right]/(2m^2)$. Beyond this value, softening is modeled both for rock-bolts and cable-bolts. Therefore, w_c^p should be large enough for cable-bolts to ensure continuous hardening (observed experimentally), as shown in Fig. 2. It is worth noting that if the parameter m is taken equal to $\pm 2n$, the maximum shear stress is reached at $\xi = w_c^p/4$ or $\xi = w_c^p$. The parameter m is used to give more flexibility to the axial behavior. Moreover, the condition $n + k > 0$ is applied to ensure the increasing trend of the failure criterion with the normal pressure.

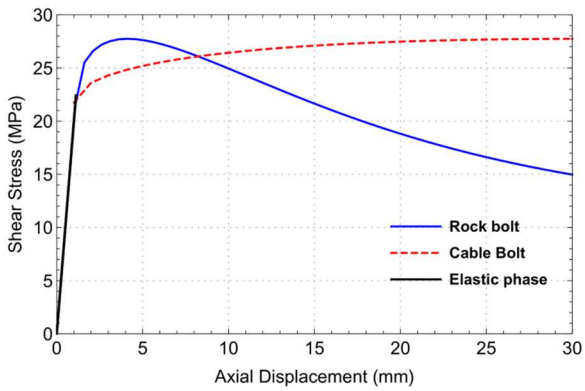

Fig. 2. Examples of shear stress (τ) for rock-bolts and cable-bolts. Parameters are K_s = 20 MPa/mm, σ_n = -5 MPa, c_r = 6 MPa, k = 1, m = 4.3, n = 2.15, and w_c^p =12 mm (rock-bolts) and w_c^p =120 mm (cable-bolts).

2.6. Radial behavior

The failure criterion and the plastic potential are different, which corresponds to a non-associated flow rule. Function $\overline{\psi}(\sigma_n, \xi)$ is given by

$$\overline{\psi}(\sigma_n, \xi) = \psi_0 \sigma_{n0} (w_c^p - 2\xi) \exp\left(-\frac{\xi}{w_c^p} - \frac{\sigma_n}{\sigma_{n0}}\right) \Big/ \left[\sqrt{\frac{\xi}{w_c^p}} 2 (w_c^p)^2\right] \quad (15)$$

The radial behavior adds a parameter to the interface model, ψ_0. The shape of this nonlinear function is inspired from experimental rock joint behavior reported by Zhao and Cai (2010) as well as Arzúa and Alejano (2013). According to Eq. (11), only the opposite of its derivative with respect to σ_n is needed:

$$\psi(\sigma_n, \xi) = \psi_0 (w_c^p - 2\xi) \exp\left(-\frac{\xi}{w_c^p} - \frac{\sigma_n}{\sigma_{n0}}\right) \Big/ \left[\sqrt{\frac{\xi}{w_c^p}} 2 (w_c^p)^2\right] \quad (16)$$

The radial opening (dilatancy) is given by the integral of Eq. (16), $u_n^p = \int \psi(\sigma_n, \xi) d\xi$. It comes that

$$u_n^p = \psi_0 \sqrt{\frac{\xi}{w_c^p}} \exp\left(-\frac{\xi}{w_c^p} - \frac{\sigma_n}{\sigma_{n0}}\right) \quad (17)$$

According to Eq. (17), dilatancy reaches its maximum for a normal stress equal to zero and is reduced when the lateral pressure increases. Parameter σ_{n0} is a reference value introduced to ensure dimensional homogeneity (usually, σ_{n0} = -1 MPa). Applying the condition given by Eq. (13) leads to $\phi \geq \psi$ for arbitrary (σ_n, ξ).

As it was mentioned earlier, the radial behavior of the interface has no elastic component. As long as the joint is not created (ξ = 0), there is no radial opening or closure. Therefore, yielding generates a plastic radial displacement ruled by the dilatancy phenomenon. As shown in Fig. 3, this radial displacement increases from zero to a maximum value attained at $\xi = w_c^p/2$. In fact, dilatancy starts at the onset of plasticity and reaches its maximum value when the joint is fully created. During a monotonic loading, further axial displacements result in joint closure, which could be due to interface material loss or an increase in normal pressure.

3. Comparison with experimental data

In order to evaluate the performance of the proposed interface model, laboratory-scale pull-out tests on cable-bolts and rock-bolts have been modeled and compared with experimental data. For this purpose, a database has been created combining results available in the literature with pull-out tests performed at the Department of Geosciences of MINES ParisTech. Some comparisons are presented in this section. We note that tests for which measurements along the axial and normal directions are available have been selected. Short embedment lengths have been chosen when possible to ensure that the shear stress is (quasi) uniform along the embedment length, so that it can be easily calculated from the axial force on the bolt (see Fig. 1), using $\tau = F/[2\pi R_b(L - u_s)]$ (L is the bolt embedment length and R_b is the bolt radius). As for the normal pressure, we use the confining pressure of the test (measured value). Indeed, many researches have proven that accessing the interface pressure requires a complex modelization of the annuli (Yacizi and Kaiser, 1992; Hyett et al., 1995; Blanco-Martín, 2012). The computed interface pressure is often overestimated, leading to a higher value of the failure criterion φ (i.e. criterion less likely reached), and to an underestimation of the interface opening. Considering the complexity of the pull-out tests (grout cracking during pull-out, untwisting of cable-bolts, etc.), and the goal of making conservative predictions, in the following the external pressure is assumed to be equal to the interface pressure. Notably, the model parameters are obtained by a simultaneous fit of the axial and radial responses. The procedure described in Section 2.3 is used, and the parameters of the model (K_s, m, n, k, c_r, w_c^p and ψ_0) are determined using the least squares method.

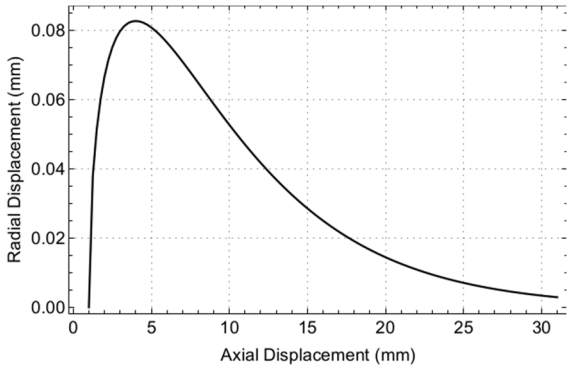

Fig. 3. Radial opening u_n (Eq. (17)). Parameters are w_c^p = 6 mm, σ_n = -1 MPa, and ψ_0 = 0.52 mm (w_c^e = 1 mm).

3.1. Comparison with pull-out tests conducted by Hyett et al. (1995)

Hyett et al. (1995) conducted a series of pull-out tests on cement-grouted seven-wire cable-bolts using three water/cement (w/c) ratios. The embedment length was L=250 mm. During the tests, the axial load and the outer radial displacement were measured. Fig. 4 compares data from Hyett et al. (1995) with the predictions of the new model, for w/c=0.4. Table 1 shows the estimated model parameters (best fit simultaneously for all tests). Overall, a good agreement between the experimental results and the model predictions can be observed. Regarding the axial response, the largest difference between experimental data and model prediction is obtained for a confinement of 5 MPa; this difference could be due to data scatter at that pressure, since the experimental curve seems too close to the curve at 10 MPa. As for the radial response, Hyett et al. (1995) stated that "*Overall, the radial displacement-axial displacement data were less consistent than the axial load-axial displacement data. This was inevitable because the measurements were made at the outer surface of a fractured cement annulus, transected by radial fractures and comprising distinct wedges able to move independently of one another during a test*". This could explain, at least partly, the differences observed between experimental data and model predictions.

Table 1. Model parameters for pull-out tests (w/c = 0.4) conducted by Hyett et al. (1995).

K_s(MPa/mm)	w_c^p(mm)	n	m	k	c_r(MPa)	ψ_0(mm)
3.5	655.24	0.86	1.72	-0.735	2	2.1

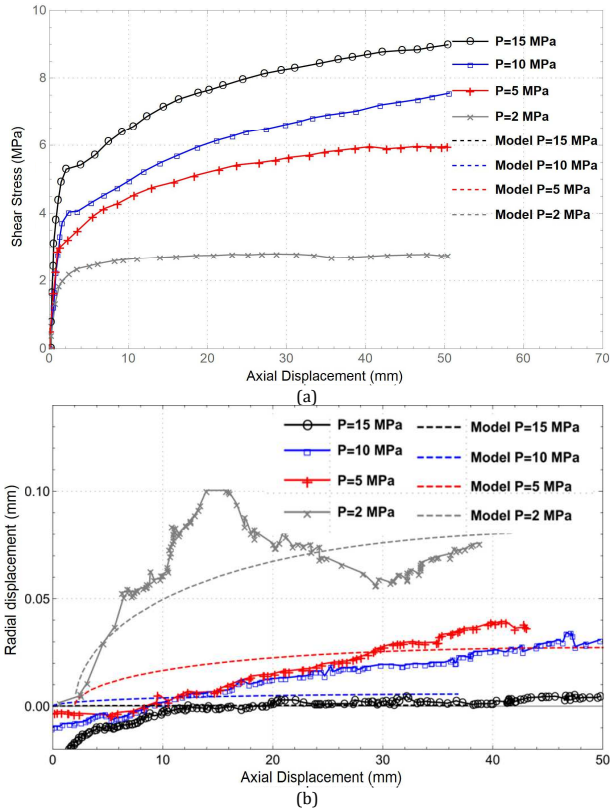

Fig. 4. Comparison between experimental data on cable-bolts (Hyett et al., 1995, w/c = 0.4) and model predictions: (a) Axial response; and (b) Radial response.

3.2. Comparison with pull-out tests conducted by Moosavi et al. (2005)

Using a similar setup, Moosavi et al. (2005) conducted a pull-out test campaign on several types of cement-grouted rock-bolts (ribbed and Dywidag bars), with embedment lengths of 100 – 150 mm. Table 2 lists the model parameters obtained to fit the pull-out tests conducted on P22 rock-bolts, and Fig. 5 compares experimental and modeled results. The comparisons are overall satisfactory.

Table 2. Model parameters for pull-out tests (P22 rock-bolts) conducted by Moosavi et al. (2005).

K_s (MPa/mm)	w_c^p (mm)	n	m	k	c_r (MPa)	ψ_0 (mm)
8	7.85	0.633	1.26	0.927	0.6	3.7

3.3. Comparison with pull-out tests conducted at MINES ParisTech

Since a research program on the topic started in 2008, around eighty pull-out tests have been carried out at the Department of Geosciences of MINES ParisTech. Fully grouted rock-bolts (smooth steel bars, ribbed bolts, and FRP) and cable-bolts (mini-cage, flexible, and IR5/IN special cable-bolts) have been tested using a bench based on the double embedment principle (Blanco-Martín, 2012; Thenevin et al., 2017). As compared to the modified Hoek cell used by Hyett et al. (1995) and Moosavi et al. (2005), the embedment length is not constant in this case, but decreases during the pull-out test. Tested embedment lengths are between 90 mm and 400 mm. Two boundary conditions can be applied on the rock sample: constant confining pressure or constant radial stiffness. Here, attention is focused on the tests performed under constant outer radial stiffness because they allow calculating the radial displacement (details can be found in Blanco-Martín, 2012).

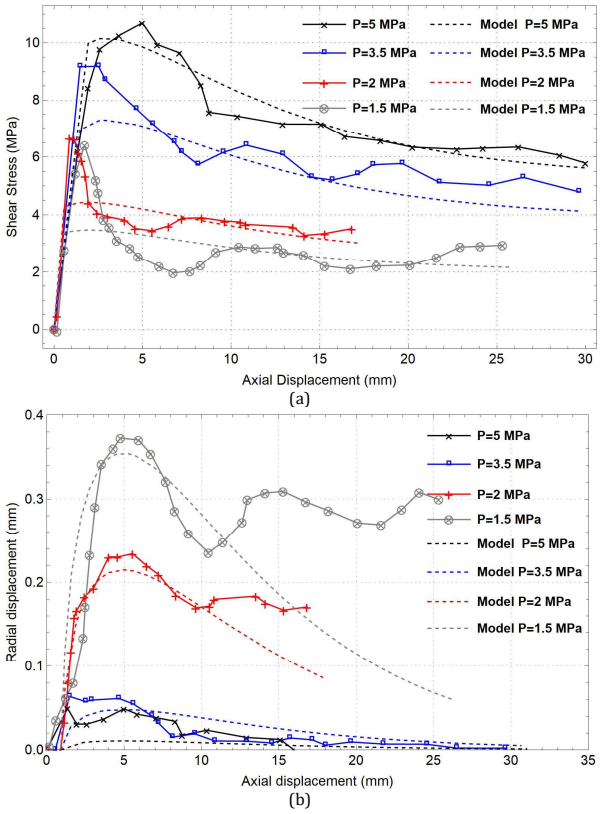

Fig. 5. Comparison between experimental data on rock-bolts (Moosavi et al., 2005, P22 rebars) and model predictions: (a) Axial response; and (b) Radial response.

Table 3 lists parameters estimated for ribbed HA25 and FRP rock-bolts, and also for flexible cable-bolts (all resin-grouted). Figs. 6-8 compare experimental results with model predictions. In these tests, the samples did not present any visual damage at the end of the pull-out process.

As it can be seen, the comparison in both the axial and the radial directions is overall satisfactory. It should be noted that in general, rock-bolts have rougher indentations than cable-bolts; as the bolt is pulled, the grouting material between and close to the indentations is damaged and sheared, particularly for high confining pressures (Blanco-Martín, 2012). This loss of grouting material may lead to interface closure under the effect of σ_n (e.g. Ghadimi et al., 2014). As shown in Fig. 8 (flexible cable-bolts), dilatancy was measured only for the radial pressure of 2.5 MPa, and for the higher lateral pressures, interface "crushing" was observed. This effect is not supported by the proposed model, considering all data deteriorated the fitting quality.

Table 3. Model parameters for pull-out tests conducted at MINES ParisTech.

Bolt type	Diameter (mm)	K_s (MPa/mm)	w_c^p (mm)	n	m	k	c_r (MPa)	ψ_0 (mm)
HA25	25	11	9.25	-0.188	6.45	0.288	4.77	2.01
FRP	25	12.5	5.56	-1.69	7.74	1.8	0.5	2.1
Flexible	23	9.5	23	1.17	3.93	-0.938	8	2.08

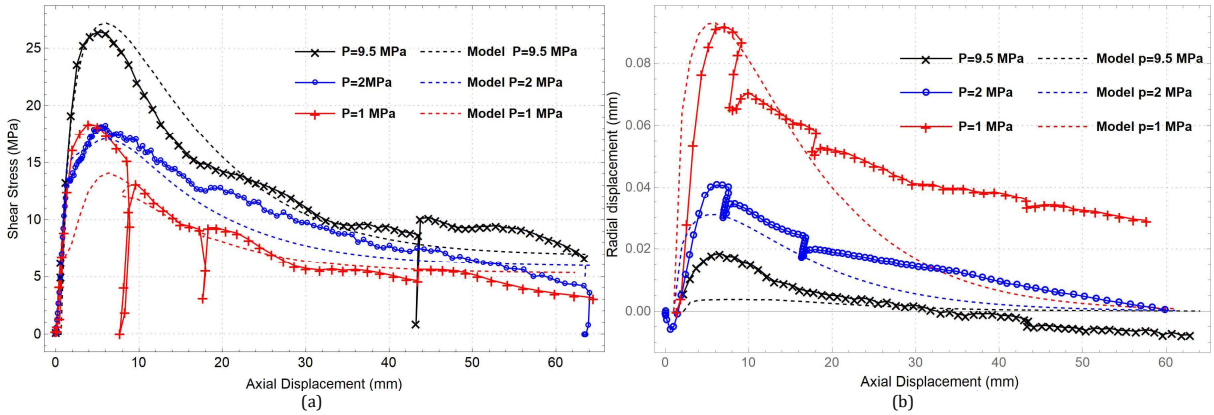

Fig. 6. Comparison between experimental data on rock-bolts (MINES ParisTech, HA25 rock-bolts) and model predictions: (a) Axial response; and (b) Radial response.

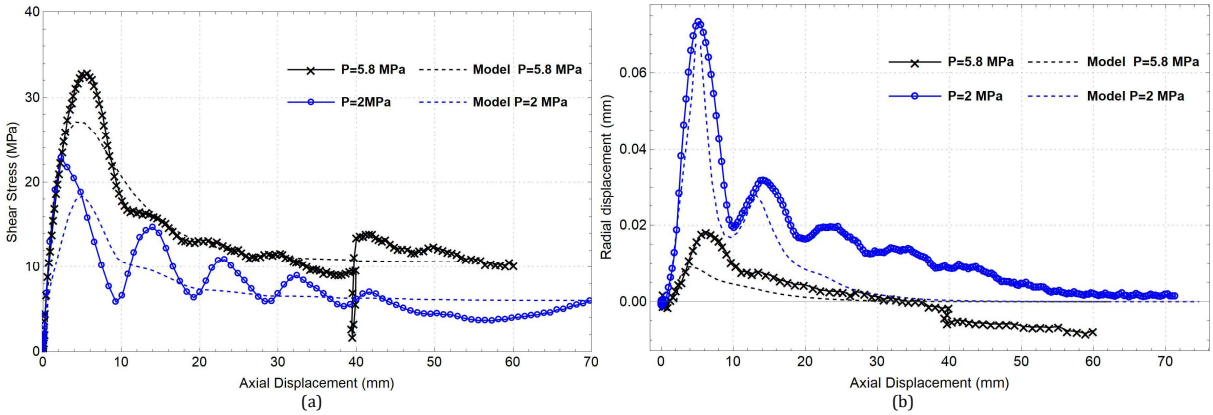

Fig. 7. Comparison between experimental data on rock-bolts (MINES ParisTech, FRP rock-bolts) and model predictions: (a) Axial response; and (b) Radial response.

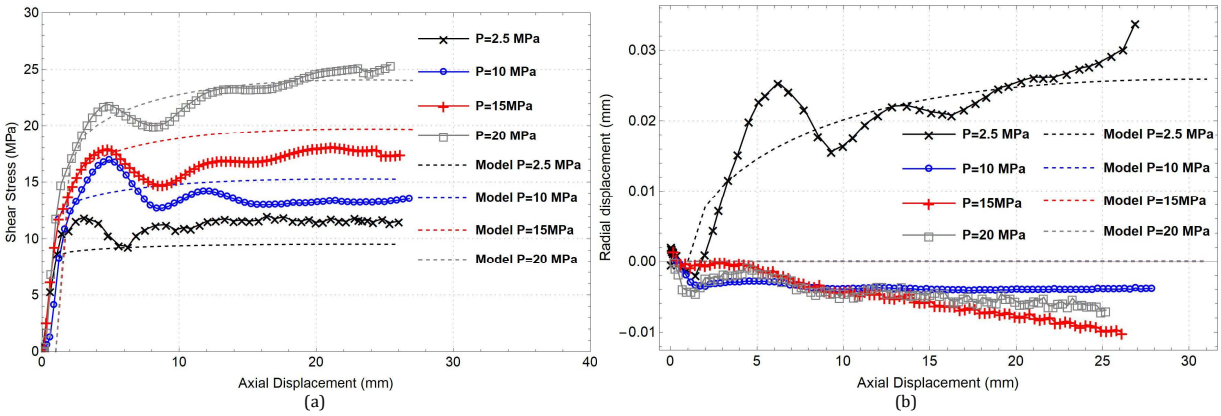

Fig. 8. Comparison between experimental data on cable-bolts (MINES ParisTech, flexible cable-bolts) and model predictions: (a) Axial response; and (b) Radial response.

Finally, it should be also noted that the experimental results reflect the bolt profile (height and angle of indentations, rib spacing, etc.); however, as geometrical effects are bolt dependent and have little importance for large-scale engineering applications, the proposed model reproduces an average response.

4. Implementation into a FEM code and modeling

The new interface constitutive model has been implemented into the two-dimensional (2D) FEM code VIPLEF, developed at the Department of Geosciences of MINES ParisTech (Tijani, 1996). In this code, the bolt itself is assumed to be elastic and can withstand axial, shear and bending loadings, with shearing occurring in the cross-section of the bar. The interface elements are linked both to the bolt and to the surrounding ground. Fig. 9 shows a schematic representation of a fully grouted bolt as implemented in VIPLEF. The interface is represented by a joint-type element at both sides of the bolt element, and comprises two series of three nodes each (second order element): one of these series is linked to the bolt, and the other is linked to the surrounding ground. The interface has no thickness. The tangential (axial) displacement of the rock mass is imposed equal at both sides of the bar. The bolt is also represented by two series of three nodes each (second order interpolation). The parameters needed to model the bolt are: cross-sectional area, Young's modulus, Poisson's ratio and the second moment of inertia with respect to the out-of-plane direction (to simulate bending).

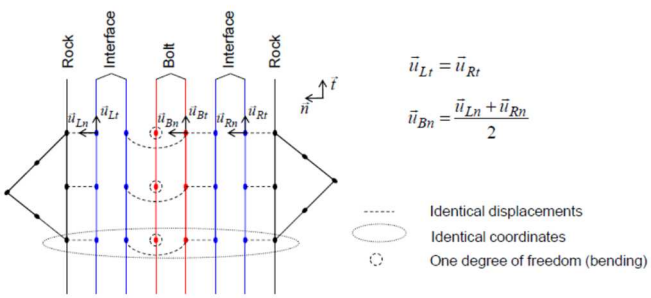

Fig. 9. Schematic representation of a fully grouted bolt in the FEM code VIPLEF.

4.1. Simulation at the elementary scale

In order to validate the implementation of the interface model, several pull-out tests have been modeled numerically at the elementary scale (i.e. bolt and interface in Fig. 9). The loading is composed of (i) a normal pressure applied along the interface elements, and (ii) an imposed axial displacement applied on the bolt.

Fig. 10 compares experimental and numerical results for three tests performed by Moosavi et al. (2005) on rock-bolts (see parameters in Table 2). As it can be seen, the numerical responses for different confining pressures are close to the experimental results. Furthermore, loading and unloading cycles were simulated to check the elastoplastic assumption of the model. At this scale, simulation of lateral behavior does not apply; it will be considered in the next section.

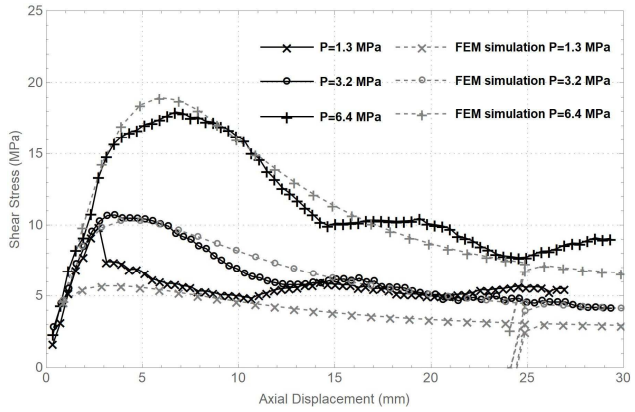

Fig. 10. Comparison between experimental data on rock-bolts (Moosavi et al., 2005) and numerical predictions at the elementary scale.

4.2. Simulation at the structural scale

The second stage for checking the numerical implementation of the new constitutive model was to simulate a laboratory test performed at MINES ParisTech including all the components of the testing bench. A pull-out test conducted on a flexible cable-bolt under a confining pressure of 2.5 MPa (Fig. 8) was selected. A 2D axisymmetric model was developed for the testing bench as illustrated in Fig. 11. All the materials were supposed to behave elastically and the interfaces between the grout and the rock and within the metallic tube to be coupled. The new interface constitutive model was applied between the bolt and the grouting material inside the rock core.

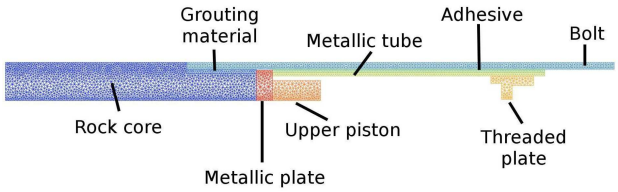

Fig. 11. FEM model used to simulate a pull-out test conducted on the testing bench of MINES ParisTech.

In order to simulate the test, a confining pressure is applied laterally on the rock sample and a relative displacement is set between the threaded plate and the biaxial cell upper piston. The displacement normal to the bottom of the rock sample is blocked.

The axial and radial responses of the numerical simulation are compared to measurements and illustrated in Fig. 12. Overall, the comparison is satisfactory, which provides confidence in the new interface law. Regarding the external radial pressure displayed (recall that the test was performed under constant radial stiffness boundary condition), a small decrease was measured during the test; this could be due to the rock sample deformation (recompaction), or to some bench parts being initially slack. Once the yield criterion is reached (dilation occurs), an increase in lateral pressure is captured both experimentally and numerically. The parameters in Table 3 were used to perform the FEM simulation. As explained previously, the interface law does not account for the bolt profile and provides an average response.

5. Discussion and conclusions

Fully grouted rock-bolts and cable-bolts often fail by a debonding mechanism that occurs at the bolt-grout interface. With the purpose of improving the current state-of-the-art, a general methodology is defined in this paper to develop rheological interface models. The methodology is used to propose a constitutive model for the bolt-grout interface, characterized by a yield criterion and a non-associated plastic potential that satisfy required thermodynamic conditions. The main originality of the new model is its capability to predict the axial and the radial behaviors of both rock-bolts and cable-bolts using a reduced number of parameters. In addition, it incorporates nonlinear radial behavior (dilatancy) after decoupling. When the interface is coupled, there is no radial relative displacement. Currently, the proposed model does not account for interface closure or bolt geometry; if needed, these limitations could be overcome in future research.

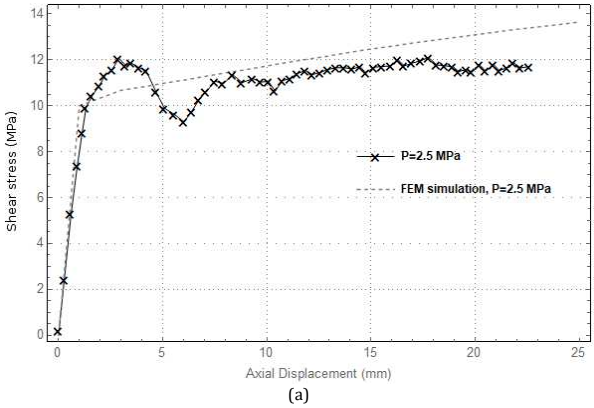

(a)

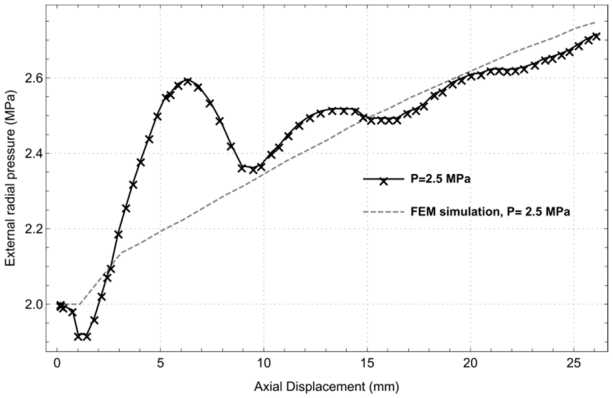

(b)

Fig. 12. Comparison between experimental data on a flexible cable-bolt and numerical predictions at the structural scale: (a) Axial response; and (b) Radial response.

A database of experimental pull-out tests has been created using results from the literature and also from tests performed at the Department of Geosciences of MINES ParisTech. Pull-out tests for which data are available both in the axial and the radial directions have been selected. This database allowed to identify the main features of the interface behavior, and served as a basis for the development and application of the new interface model. The agreement between experimental and modeled pull-out responses is quite satisfactory, which provides confidence in the ability of the proposed model to reproduce the response of fully grouted bolts under axial loads.

The new model has been implemented in the in-house FEM code VIPLEF, and simulations of pull-out tests under different confining pressures have been performed and successfully compared with experimental results. The simulations have been performed at the elementary and the structural scales. The positive results obtained during this research encourage the use of the new interface model for bolting support design and optimization in underground engineering applications as the next step, such as in Cui et al. (2019b).

Declaration of competing interest

The authors wish to confirm that there are no known conflicts of interests associated with this publication and there has been no significant financial support for this work that could have influenced its outcome.

Acknowledgments

This research has been supported by the Research Fund for Coal and Steel (RFCS) in the context of the European project Advancing Mining Support Systems to Enhance the Control of Highly Stressed Ground (AMSSTED). The authors would like to thank the European Research Commission as well as the partners involved in this project.

List of symbols

K_s	Shear stiffness
K_n	Normal stiffness
$\varphi(\sigma, \xi)$	Failure function
u_n	Normal displacement
u_s	Tangential displacement
u^p	Plastic displacement
u_n^p	Plastic normal displacement
u_s^p	Plastic tangential displacement
ξ	Internal variable (plastic tangential displacement)
$\overset{r}{s}$	Interface stress vector
σ_n	Normal stress
τ	Shear stress
$\psi(\sigma_n, \xi)$	Dilatancy function
c_r	Residual cohesion
w_c^e	Elastic displacement limit
w_c^p	Critical plastic tangential displacement
R_b	Bolt radius
R_g	Borehole radius
R_r	Rock/soil sample outer radius
p_{conf}	Confining pressure
F	Axial force on the bolt
w^p	Plastic work

References

Alejano LR, Alonso E. Considerations of the dilatancy angle in rocks and rock masses. International Journal of Rock Mechanics and Mining Sciences 2005;42(4):481-507.

Arzúa J, Alejano LR. Dilation in granite during servo-controlled triaxial strength tests. International Journal of Rock Mechanics and Mining Sciences 2013;61:43-56.

Barton NR, Bandis S. Review of predictive capabilities of JRC-JCS model in engineering practice. In: Proceedings of the International Symposium on Rock Joints, Balkema, Rotterdam,1990; 603–10.

Benmokrane B, Chennouf A, Mitri HS. Laboratory evaluation of cement-based grouts and grouted rock anchors. International Journal of Rock Mechanics and Mining Sciences & Geomechanics Abstracts 1995;32(7):633-42.

Blanco-Martín L, Tijani M, Hadj-Hassen F. A new analytical solution to the mechanical behaviour of fully grouted rockbolts subjected to pull-out tests. Construction and Building Materials 2011;25(2):749-55.

Blanco-Martín L. Theoretical and experimental study of fully grouted rockbolts and cablebolts under axial loads. PhD Thesis. MINES ParisTech; 2012.

Blanco-Martín L, Tijani M, Hadj-Hassen F, Noiret A. Assessment of the bolt-grout interface behaviour of fully grouted rockbolts from laboratory experiments under axial loads. International Journal of Rock Mechanics and Mining Sciences 2013;63:50-61.

Blanco-Martín L, Tijani M, Hadj-Hassen F, Noiret A. Boulonnage à ancrage réparti: étude de l'interface barre-scellement sous sollicitations axiales. Revue Française de Géotechnique 2016;146:1-11 (in French).

Cai Y, Esaki T, Jiang YJ. A rock bolt and rock mass interaction model. International Journal of Rock Mechanics and Mining Sciences 2004;41:1055-67.

Carol I, Prat PC, López CM. Normal/shear cracking model: application to discrete crack analysis. Journal of Engineering Mechanics 1997;123(8):765-73.

Chakrabarty J. Theory of plasticity. 3rd edition. Butterworth-Heinemann, 2006.

Chen SH, Zhang X, Shahrour I. Composite element model for the bonded anchorage head of stranded wire cable in tension. International Journal for Numerical and Analytical Methods in Geomechanics 2015a;39:1352-68.

Chen JH, Saydam S, Hagan PC. An analytical model of the load transfer behavior of fully grouted cable bolts. Construction and Building Materials 2015b;101:1006-15.

Cui L, Dong YK, Sheng Q. Shen Q. New numerical procedures for fully-grouted bolt in the rock mass with slip and non-slip cases at the rock-bolt interface. Construction and Building Materials 2019a;204:849-63.

Cui L, Zheng JJ, Sheng Q, Pan Y. A simplified procedure for the interaction between fully-grouted bolts and rock mass for circular tunnels. Computers and Geotechnics 2019b,106: 177-192.

Ghadimi M, Shahriar K, Jalalifar H. Analysis profile of the fully grouted rock bolt in jointed rock using analytical and numerical methods. International Journal of Mining Science and Technology 2014;24(5):609-15.

He L, An XM, Zhao ZY. Fully grouted rock bolts: an analytical investigation. Rock Mechanics and Rock Engineering 2014;48:1181-96.

Hill R. A variational principle of maximum plastic work in classical plasticity. The Quarterly Journal of Mechanics and Applied Mathematics 1948;1:18–28.

Hyett AJ, Bawden WF, Reicher RD. The effect of rock mass confinement on the bond strength of fully grouted cable bolts. International Journal of Rock Mechanics and Mining Sciences & Geomechanics Abstracts 1992;29(5):503-24.

Hyett AJ, Bawden WF, Macsporran GR, Moosavi M. A constitutive law for bond failure of fully-grouted cable bolts using a modified Hoek cell. International Journal of Rock Mechanics and Mining Sciences & Geomechanics Abstracts 1995;32(1):11-36.

Indraratna B, Thirukumaran S, Brown ET, Zhu SP. Modelling the shear behaviour of rock joints with asperity damage under constant normal stiffness. Rock Mechanics and Rock Engineering 2015;48:179-95.

Khan AS, Huang SJ. Continuum theory of plasticity. New York: John Wiley & Sons, 1995.

Ladanyi B, Archambault G. Direct and indirect determination of shear strength of rock mass. AIME Annual Meeting, Las Vegas. 1980; p.16.

Li C, Stillborg B. Analytical models for rock bolts. International Journal of Rock Mechanics and Mining Sciences 1999; 36(8):1013-29.

Li DQ, Masoumi H, Saydan S, Hagan PC. A constitutive model for load-displacement performance of modified cable bolts. Tunnelling and Underground Space Technology 2017;68:95-105.

Li C. Principles of rockbolting design. Journal of Rock Mechanics and Geotechnical Engineering 2017;9(3):396-414.

Lubliner J. Plasticity theory. 3rd edition. Mineola, USA: Dover Publications, 2008.

Ma S. Zhao Z, Nie W, Gui Y. A numerical model of fully grouted bolts considering the tri-linear shear bond–slip model. Tunn. Undergr. Space Technol., 2016; 54, 73-80.

Moosavi M, Jafari A, Khosravi A. Bond of cement grouted reinforcing bars under constant radial pressure. Cement and Concrete Composites 2005;27(1):103-9.

Nairn JA. Generalized shear-lag analysis including imperfect interfaces. Advanced Composites Letters 2004;13(6):263-74.

Oh J, Cording EJ, Moon T. A joint shear model incorporating small-scale and large-scale irregularities. International Journal of Rock Mechanics and Mining Sciences 2015;76: 78-87.

Plesha ME. Constitutive models for rock discontinuities with dilatancy and surface degradation. International Journal for Numerical and Analytical Methods in Geomechanics 1987;11:345-62.

Pouya A. Yazdi BP. A damage-plasticity model for cohesive fractures. International Journal of Rock Mechanics and Mining Sciences 2015;73:194-202.

Ren FF, Yang ZJ, Chen JF, Chen WW. An analytical analysis of the full-range behaviour of grouted rockbolts based on a tri-linear bond-slip model. Construction and Building Materials 2010;24(3):361-70.

Renani HR, Martin CD. Cohesion degradation and friction mobilization in brittle failure of rocks. International Journal of Rock Mechanics and Mining Sciences 2018;106:1-13.

Saeb S, Amadei B. Modelling rock joints under shear and normal loading. International Journal of Rock Mechanics and Mining Sciences & Geomechanics Abstracts 1992;29(3):267-78.

Stillborg B. Professional users handbook for rock bolting. Clausthal-Zellerfeld: Trans Tech Publ, 1986.

Thenevin I, Blanco-Martín L, Hadj-Hassen F, Schleifer J, Lubosik Z, Wrana A. Laboratory pull-out tests on fully grouted rock bolts and cable bolts: Results and lessons learned. Journal of Rock Mechanics and Geotechnical Engineering 2017;9(5):843-55.

Tian HM, Chen WZ, Yang DS, Yang JP. Experimental and numerical analysis of the shear behavior of cemented concrete-rock joints. Rock Mechanics and Rock Engineering 2015; 48:213-22.

Tijani M. Short description of VIPLEF code. In: Stephanson O, Jing L, Tsang CF, editors. Coupled thermo-hydro-mechanical processes of fractured media, Vol. 79. Amsterdam: Elsevier, 1996. p. 507–11.

Windsor C, Thompson A. Terminology in rock reinforcement practice. In: Aubertin M, Hassani F, Mitri H, editors. Rock Mechanics: Tools and Techniques, Proceedings of the 2nd North American Rock Mechanics Symposium. Rotterdam: A.A. Balkema, 1996. p. 225-32.

Yacizi S, Kaiser PK. Bond strength of grouted cable-bolts. International Journal of Rock Mechanics and Mining Sciences & Geomechanics Abstracts 1992;29:279-92.

Zhao XG, Cai M. A mobilized dilatation angle model for rocks. International Journal of Rock Mechanics and Mining Sciences 2010;47(3):368-84.

Dr. Emad Jahangir is a researcher-lecturer at Department of Geosciences of MINES ParisTech. His research interests cover soil and rock mechanics, and their interactions with surrounding structures within coupled THM processes.